

Distinctive Collider Signals for a Two Higgs Triplet Model

Dilip Kumar Ghosh^{a,1}, Nivedita Ghosh^{a,2}, Biswarup Mukhopadhyaya^{b,3}

^a*School Of Physical Sciences, Indian Association for the Cultivation of Science,
2A & 2B, Raja S.C. Mullick Road, Kolkata 700032, India*

^b*Regional Centre for Accelerator-based Particle Physics
Harish-Chandra Research Institute*

Abstract

The extension of the Standard Model (SM) with two complex $SU(2)_L$ scalar triplets enables one to have the Type II seesaw mechanism operative consistently with texture-zero neutrino mass matrices. This framework predicts additional doubly charged, singly charged and neutral spinless states. We show that, for certain values of the model parameters, there is sufficient mass splitting between the two doubly charged states ($H_1^{\pm\pm}, H_2^{\pm\pm}$) that allows the decay $H_1^{\pm\pm} \rightarrow H_2^{\pm\pm} h$, and thus leads to a unique signature of this scenario. We show that the final state $2(\ell^\pm \ell^\pm) + 4b + E_T$ arising from this mode can be observed at the high energy, high luminosity (HE-HL) run of the 14 TeV Large Hadron Collider (LHC), and also at a 100 TeV Future Circular Collider (FCC-hh).

I Introduction

A 125 GeV scalar, with a striking resemblance to the Higgs boson proposed in the Standard Model(SM) has been observed at the Large Hadron Collider(LHC) [1, 2]. In spite of being a very successful phenomenological theory, the SM, however, cannot generate neutrino masses as suggested in various observations [3–5]. A popular set of mechanisms for generating such masses are the three types of seesaw mechanism [6–15]. Their experimental confirmation, on accelerators in particular are also of considerable interest [16–21]. Out of the three suggested types of seesaw, Type II involves an extension of the scalar sector with an additional complex $SU(2)_L$ triplet scalar with hypercharge $Y = 2$. This triplet couples to leptons via interactions which violate lepton number by two units [9–13, 22, 23] and thus generates Majorana masses for neutrinos.

The most striking phenomenological consequence of such a triplet scalar is the presence of a doubly charged scalar. The triplet vacuum expectation value (vev), denoted here by w , is rather tightly constrained by the ρ -parameter to values less than about 5 GeV [24]. The doubly charged scalar can decay either to produce same-sign dilepton peaks for $w < 10^{-4}$ GeV, or to same-sign W -pairs for $w > 10^{-4}$ GeV [25–27]. A rather strong lower limit of 770 - 800

¹tpdkg@iacs.res.in

²tpng@iacs.res.in (Corresponding author)

³biswarup@hri.res.in

GeV exists on the doubly charged scalar mass in the former case, from same-sign dilepton searches at the LHC [28]. There is no such bound yet on doubly charged scalar mass for $w > 10^{-4}$ GeV [29]. This is because (a) a relatively large triplet vev implies small $\Delta L = 2$ Yukawa couplings from a consideration of neutrino masses, and (b) overcoming standard model (SM) backgrounds for the final state driven by same-sign W-pairs is a challenging task, and requires a large integrated luminosity. Several works can be found in the literature, dwelling on strategies for unraveling the triplet scenario, both before [18–21, 30–32] and after [33–42] the discovery of the 125 GeV scalar.

From some special angles, however, a single triplet is inadequate for consistent neutrino mass generation in the Type-II seesaw model. For example, the somewhat different mass and mixing patterns in the neutrino sector (as compared to those in the quark sector) calls for studies in neutrino mass matrix models. One class of such models consists of zero textures, having some vanishing entries in the mass matrix, thus leading to relations between mass eigenvalues and mixing angles, and ensuring better predictiveness in the neutrino sector. It has been shown, that zero textures are inconsistent with Type-II seesaw models with a single scalar triplet [43]. Such inconsistency is removed when one has two such triplets, as has been demonstrated in [44]. This of course opens up the possibility of new collider signals which has been only partially investigated.

In this work, we study the LHC signals that can decidedly tell us about the existence of two complex triplet scalars (Δ_1, Δ_2). For example, in [44] searches via $\Delta_1^{\pm\pm} \rightarrow \Delta_2^\pm W^\pm$ decay mode have been discussed. It should be noted that such a decay is disfavored in the single-triplet scenario, since the ρ -parameter restricts the mass splitting among fields having different electric charges. Another decay channel that opens up in this scenario is $\Delta_1^{\pm\pm} \rightarrow \Delta_2^{\pm\pm} h$, h being the SM-like Higgs. As has been shown in [45], this mode prevails especially in the presence of at least one CP-violating phase.

We neglect CP-violating phases in the present study. Regions of the parameter space answering to both $\Delta_1^{\pm\pm} \rightarrow \Delta_2^\pm W^\pm$ and $\Delta_1^{\pm\pm} \rightarrow \Delta_2^{\pm\pm} h$ have been identified, and the corresponding signals have been predicted. Both these channels can lead to the final state $2\ell^\pm \ell^\pm + 4b + \cancel{E}_T$, where, $\ell \equiv e, \mu$. We carry out a detailed analysis to estimate signal significance of this scenario in the regions of the parameter space, consistent with all current limits both at the high energy high-luminosity (HE-HL) run of the LHC with $\sqrt{s} = 14$ TeV and at the proposed $\sqrt{s} = 100$ TeV Future Circular Collider (FCC-hh) at CERN [46] or the Super Proton-Proton Collider (SPPC) in China [47]. Further details on the physics potential of the 100 TeV collider can be found, for example, in [48]. We also comment on how to differentiate the two-triplet scenario from a single-triplet one using the signal analysis in this work.

The paper is organized as follows. In Section II we discuss a little bit about the well-motivated $Y = 2$ single triplet scenario. Relevant phenomenological features of the two-triplet scenario are presented in Section III. Results of the collider analysis are reported in Section IV. We summarize and conclude in Section V.

II The $Y = 2$ single triplet scenario

In this section we briefly describe the single triplet scenario. Along with the SM fields, there is an extra $SU(2)_L$ complex triplet scalar field Δ with hypercharge $Y = 2$.

$$\Delta = \frac{\sigma^i}{\sqrt{2}} \Delta_i = \begin{pmatrix} \delta^+/\sqrt{2} & \delta^{++} \\ \delta^0 & -\delta^+/\sqrt{2} \end{pmatrix}, \quad (1)$$

where $\Delta_1 = (\delta^{++} + \delta^0)/\sqrt{2}$, $\Delta_2 = i(\delta^{++} - \delta^0)/\sqrt{2}$, $\Delta_3 = \delta^+$.

The vevs of the doublet and the triplet are given by

$$\langle \phi \rangle_0 = \frac{1}{\sqrt{2}} \begin{pmatrix} 0 \\ v \end{pmatrix} \quad \text{and} \quad \langle \Delta \rangle_0 = \begin{pmatrix} 0 & 0 \\ w & 0 \end{pmatrix}, \quad (2)$$

respectively and the electroweak vev is given by $v = \sqrt{v^2 + 2w^2} = 246$ GeV.

The most general scalar potential involving ϕ and Δ can be written as

$$\begin{aligned} V(\phi, \Delta) = & a \phi^\dagger \phi + \frac{b}{2} \text{tr}(\Delta^\dagger \Delta) + c (\phi^\dagger \phi)^2 + \frac{d}{4} (\text{tr}(\Delta^\dagger \Delta))^2 \\ & + \frac{r}{2} \phi^\dagger \phi \text{tr}(\Delta^\dagger \Delta) + \frac{f}{4} \text{tr}(\Delta^\dagger \Delta^\dagger) \text{tr}(\Delta \Delta) \\ & + h \phi^\dagger \Delta^\dagger \Delta \phi + \left(t \phi^\dagger \Delta \tilde{\phi} + \text{H.c.} \right), \end{aligned} \quad (3)$$

where $\tilde{\phi} \equiv i\tau_2 \phi^*$. In general, both v and w can be complex. However, since we want to avoid all CP-violating effects, we choose both the vevs to be real and positive, which as a result implies that t has to be real.

It should be remembered that the choice $a < 0$, $b > 0$ ensures the primary source of spontaneous symmetry breaking to be the vev of the scalar doublet. At the same time, the ρ -parameter has to be very close to its tree-level SM value of unity, as required by the latest data, namely, $\rho = 1.0004_{-0.0004}^{+0.0003}$ [49] for $w \ll v$. Also the doublet-triplet mixing has to be small and the perturbativity of all quartic couplings at the electroweak scale has to be guaranteed.

All the aforementioned constraints drive us to choose the following orders of magnitude for the parameters in the potential:

$$a, b \sim v^2; \quad c, d, r, f, h \sim 1; \quad |t| \ll v. \quad (4)$$

The mass terms for singly-charged scalars in this model are given by

$$\mathcal{L}_S^\pm = -(H^-, \phi^-) \mathcal{M}_+^2 \begin{pmatrix} H^+ \\ \phi^+ \end{pmatrix} \quad (5)$$

where

$$\mathcal{M}_+^2 = \begin{pmatrix} (q + h/2)v^2 & \sqrt{2}v(t - wh/2) \\ \sqrt{2}v(t - wh/2) & 2(q + h/2)w^2 \end{pmatrix} \quad \text{and} \quad q = \frac{|t|}{w}. \quad (6)$$

Diagonalization of the matrix should yield one zero eigenvalue, corresponding to the Goldstone boson. The singly-charged mass-squared matrix is

$$m_{\Delta^+}^2 = \left(q + \frac{h}{2} \right) (v^2 + 2w^2), \quad (7)$$

whereas the doubly-charged scalar mass is

$$m_{\Delta^{++}}^2 = (h + q)v^2 + 2fw^2. \quad (8)$$

In the limit $w \ll v$, one obtains

$$m_{\Delta^{++}}^2 - m_{\Delta^+}^2 \simeq \frac{h}{2}v^2. \quad (9)$$

Electroweak precision data imply $\Delta M \equiv |m_{\Delta^{++}} - m_{\Delta^+}| \lesssim 50$ GeV [50, 51] assuming a light SM Higgs boson of mass $m_h = 125$ GeV and top quark mass $M_t = 173$ GeV. Hence, the decay mode $\Delta^{++} \rightarrow \Delta^+ W^+$ is kinematically not allowed with a single triplet scalar.

III Extension with two triplets

The single-triplet scenario can sometimes turn out to be inadequate. For example, the somewhat novel kind of bi-large mixing in the neutrino sector motivates people to link such a mixing pattern with the neutrino mass matrix itself. The number of arbitrary parameters in such an investigation is reduced, and the mass eigenvalues and mixing angles are linked in a predictive manner, if some elements of this matrix vanish. It is with this in view that various texture zero neutrino mass matrices have been proposed, for example, through the imposition of certain Abelian symmetries. Two-zero textures constitute a popular subset of such models, which have been widely used in various contexts [43, 52–65].

In the specific context of Type II seesaw, however, inconsistencies arise when texture zeros (especially two-zero textures) are attempted [66]. Such inconsistency can be avoided, as already mentioned, when two scalar triplets are present. In such a scenario, one extends the SM with two $Y = 2$ triplet scalars Δ_1, Δ_2 :

$$\Delta_1 = \begin{pmatrix} \delta_1^+ & \sqrt{2}\delta_1^{++} \\ \sqrt{2}\delta_1^0 & -\delta_1^+ \end{pmatrix} \quad \text{and} \quad \Delta_2 = \begin{pmatrix} \delta_2^+ & \sqrt{2}\delta_2^{++} \\ \sqrt{2}\delta_2^0 & -\delta_2^+ \end{pmatrix}. \quad (10)$$

The vevs of the scalar triplets are given by

$$\langle \Delta_1 \rangle_0 = \begin{pmatrix} 0 & 0 \\ w_1 & 0 \end{pmatrix} \quad \text{and} \quad \langle \Delta_2 \rangle_0 = \begin{pmatrix} 0 & 0 \\ w_2 & 0 \end{pmatrix}. \quad (11)$$

The scalar potential in this scenario involving the Higgs doublet and the two triplets can be

written as

$$\begin{aligned}
V(\phi, \Delta_1, \Delta_2) = & \\
& a \phi^\dagger \phi + \frac{1}{2} b_{kl} \text{tr}(\Delta_k^\dagger \Delta_l) + c(\phi^\dagger \phi)^2 + \frac{1}{4} d_{kl} \left(\text{tr}(\Delta_k^\dagger \Delta_l) \right)^2 \\
& + \frac{1}{2} r_{kl} \phi^\dagger \phi \text{tr}(\Delta_k^\dagger \Delta_l) + \frac{1}{4} f_{kl} \text{tr}(\Delta_k^\dagger \Delta_l^\dagger) \text{tr}(\Delta_k \Delta_l) \\
& + h_{kl} \phi^\dagger \Delta_k^\dagger \Delta_l \phi + g \text{tr}(\Delta_1^\dagger \Delta_2) \text{tr}(\Delta_2^\dagger \Delta_1) + g' \text{tr}(\Delta_1^\dagger \Delta_1) \text{tr}(\Delta_2^\dagger \Delta_2) \\
& + \left(t_k \phi^\dagger \Delta_k \tilde{\phi} + \text{H.c.} \right), \tag{12}
\end{aligned}$$

where $k, l = 1, 2$.

As mentioned in the previous section, v, w_1, w_2 as well as t_1, t_2 are taken to be real and positive. One can also use for illustration, without any loss in the generality of the results,

$$a, b_{kl} \sim v^2; \quad c, d_{kl}, r_{kl}, h_{kl}, f_{kl}, g, g' \sim \mathcal{O}(1); \quad |t_k| \ll v. \tag{13}$$

With $w_1, w_2 \ll v$.

We redefine the following 2×2 matrices and vectors:

$$B = (b_{kl}), \quad E = (r_{kl} + h_{kl}), \quad H = (h_{kl}), \quad t = \begin{pmatrix} t_1 \\ t_2 \end{pmatrix}, \quad w = \begin{pmatrix} w_1 \\ w_2 \end{pmatrix}. \tag{14}$$

The minimization of the potential (12), neglecting all terms quartic in the triplet vevs, yields

$$\left(B + \frac{v^2}{2} (E - H) \right) w + v^2 t = 0, \tag{15}$$

$$a + cv^2 + \frac{1}{2} w^T (E - H) w + 2t \cdot w = 0, \tag{16}$$

where we have used $t \cdot w = \sum_k t_k w_k$. Solving Eq. (15) and Eq. (16) simultaneously, $w_k (k = 1, 2)$ are obtained as

$$w = -v^2 \left(B + \frac{1}{2} v^2 (E - H) \right)^{-1} t. \tag{17}$$

After diagonalization of different kinds of scalar mass matrices following electroweak symmetry breaking (EWSB), we obtain the charged scalars ($H_1^{\pm\pm}, H_2^{\pm\pm}$), singly charged Higgs (H_1^\pm, H_2^\pm), and the neutral CP-even (h, H_1, H_2) and CP-odd (A_1, A_2) scalars. Among them h is the SM-like Higgs.

The mass matrix of the doubly-charged scalars is given by

$$\mathcal{M}_{\pm\pm}^2 = B + \frac{v^2}{2} (E + H). \tag{18}$$

which can be diagonalized by

$$U^\dagger \mathcal{M}_{\pm\pm}^2 U = \text{diag}(M_1^2, M_2^2) \tag{19}$$

yielding the mass eigenstates:

$$\begin{pmatrix} \delta_1^{\pm\pm} \\ \delta_2^{\pm\pm} \end{pmatrix} = U \begin{pmatrix} H_1^{\pm\pm} \\ H_2^{\pm\pm} \end{pmatrix} \quad (20)$$

The singly charged scalar mass-squared matrix comes from

$$-\mathcal{L}_S^\pm = (\delta_1^-, \delta_2^-, \phi^-) \mathcal{M}_\pm^2 \begin{pmatrix} \delta_1^+ \\ \delta_2^+ \\ \phi^+ \end{pmatrix} + \text{H.c.}, \quad (21)$$

where

$$\mathcal{M}_\pm^2 = \begin{pmatrix} B + \frac{v^2}{2} E & \sqrt{2}v(t - Hw/2) \\ \sqrt{2}v(t - Hw/2)^\dagger & a + cv^2 + \frac{1}{2}w^T(E + H)w \end{pmatrix}. \quad (22)$$

Using equations (15) and (16) we get,

$$\mathcal{M}_\pm^2 \begin{pmatrix} v_T \\ v/\sqrt{2} \end{pmatrix} = 0. \quad (23)$$

This serves as a consistency check that the singly charged mass matrix has to have an eigenvector with zero eigenvalue that corresponds to the would-be-Goldstone boson.

It is evident from Eq. (13) that b is of the order of v^2 . Therefore, in a rough approximation one can safely ignore the t_k and the triplet vevs in the mass matrix \mathcal{M}_\pm^2 . In that limit, also $a + cv^2 = 0$ and the charged would-be-Goldstone boson is equivalent to ϕ^\pm . There is no mixing with the δ_k^\pm .

The singly charged mass matrix can be diagonalized by

$$V^\dagger \mathcal{M}_\pm^2 V = \text{diag}(\mu_1^2, \mu_2^2, 0), \quad (24)$$

with

$$\begin{pmatrix} \delta_1^\pm \\ \delta_2^\pm \\ \phi^\pm \end{pmatrix} = V \begin{pmatrix} H_1^\pm \\ H_2^\pm \\ G^\pm \end{pmatrix}. \quad (25)$$

Where G^\pm is the charged would-be-Goldstone boson.

Interactions with the W-boson are given by

$$\begin{aligned} \mathcal{L}_{\text{gauge}} &= ig \sum_{k=1}^2 [\delta_k^- (\partial^\mu \delta_k^{++}) - (\partial^\mu \delta_k^-) \delta_k^{++}] W_\mu^- \\ &\quad - \frac{g^2}{\sqrt{2}} \sum_{k=1}^2 w_k W_\mu^- W^{-\mu} \delta_k^{++} + \text{H.c.} \end{aligned} \quad (26)$$

Here g is the $SU(2)_L$ gauge coupling constant. Changing the gauge basis into mass basis allows us to compute the decay rates of $H_1^{++} \rightarrow H_2^+ W^+$ and $H_k^{++} \rightarrow W^+ W^+$ ($k = 1, 2$).

The ($\Delta L = 2$) Yukawa interaction Lagrangian involving the triplets and the leptons is

$$\mathcal{L}_Y = \frac{1}{2} \sum_{k=1}^2 h_{ij}^{(k)} L_i^T C^{-1} i\tau_2 \Delta_k L_j + \text{H.c.}, \quad (27)$$

where L_i denote the left-handed lepton doublets, C is the Dirac charge conjugation matrix, the $h_{ij}^{(k)}$ are the symmetric neutrino Yukawa coupling matrices of the triplets Δ_k , and the $i, j = 1, 2, 3$ are the summation indices over the three neutrino flavours.¹

When the triplets acquire vev from Eq. (27) one can generate the neutrino mass matrix as :

$$(M_\nu)_{ij} = h_{ij}^{(1)} w_1 + h_{ij}^{(2)} w_2. \quad (28)$$

This connects the Yukawa coupling constants $h_{ij}^{(1)}$, $h_{ij}^{(2)}$ and the triplet vevs w_1 , w_2 .

In this work we use, once more as illustration, the normal hierarchy of the neutrino mass spectrum and set the lowest neutrino mass eigenvalue to zero. The elements of The neutrino mass matrix M_ν can be obtained by using the observed central values of the various lepton mixing angles and by diagonalising as

$$M_\nu = U \hat{M}_\nu U^\dagger, \quad (29)$$

where U is the PMNS matrix given by [67]

$$U = \begin{pmatrix} c_{12}c_{13} & s_{12}c_{13} & s_{13}e^{-i\delta} \\ -s_{12}c_{23} - c_{12}s_{23}s_{13}e^{i\delta} & c_{12}c_{23} - s_{12}s_{23}s_{13}e^{i\delta} & s_{23}c_{13} \\ s_{12}s_{23} - c_{12}c_{23}s_{13}e^{i\delta} & -c_{12}s_{23} - s_{12}c_{23}s_{13}e^{i\delta} & c_{23}c_{13} \end{pmatrix} \quad (30)$$

and \hat{M}_ν is the diagonal matrix of the neutrino masses. We have dropped possible Majorana phases for simplicity. Global analyses of data can be used to resolve the various entries of U [68]. The left-hand side of Eq. (28) is reliably represented, at least in orders of magnitude, by the central values of all angles, including that for θ_{13} as obtained from the recent Daya Bay and RENO experiments [69, 70]. The actual mass matrix thus constructed has some elements at least one order of magnitude smaller than the others, thus suggesting texture zeros.

IV Analysis

Let us now look for smoking gun collider signals of doubly charged scalars of this scenario with $w_k \sim \mathcal{O}(1)$ GeV. The spectacular $l^\pm l^\pm$ decay channels are suppressed in this case. The doubly charged scalars now mainly decay into the following final states:

$$H_1^{\pm\pm} \rightarrow H_2^{\pm\pm} h, \quad (31)$$

$$H_1^{\pm\pm} \rightarrow W^\pm W^\pm, \quad (32)$$

$$H_1^{\pm\pm} \rightarrow H_2^\pm W^\pm, \quad (33)$$

$$H_2^{\pm\pm} \rightarrow W^\pm W^\pm. \quad (34)$$

¹We assume the charged-lepton mass matrix to be already diagonal.

The decay mode as mentioned in Eq.(31) is absent in the single-triplet model, since there is only one doubly charged scalar particle. Also, the equivalent of Eq.(33), namely, $H_1^{\pm\pm} \rightarrow H_1^\pm W^\pm$ is kinematically disfavored since the mass splitting between singly and doubly charged scalar is restricted by the ρ parameter constraint [49–51]. Hence, in order to distinguish between the single triplet and the double triplet scalar model, it is advantageous to investigate channels in Eq.(31) and Eq.(33), since the corresponding event topologies cannot be faked by a single-triplet scenario. The production of W^\pm in association with the SM-like Higgs boson leads to the following final state:

$$2\ell^\pm\ell^\pm + 4b + \cancel{E}_T. \quad (35)$$

where $\ell = e, \mu$, which arise from $W^\pm \rightarrow \ell^\pm\nu_\ell(\bar{\nu}_\ell)$ and $h \rightarrow b\bar{b}$ decay modes.

Since the doublet-triplet mixing is small in this model, there is no noticeable difference in production rate in the gluon fusion channel and also the tree-level decay of the SM-like Higgs. However, the presence of $H_1^{\pm\pm}, H_2^{\pm\pm}$ and H_1^\pm, H_2^\pm modify the loop-induced $h \rightarrow \gamma\gamma$ decay significantly. Detailed analyses of such modification can be found in [24, 50, 71–75]. Here we just ensure that our benchmark points are consistent with the limits on the diphoton signal strength of the Higgs at the 2σ level [76].

IV.1 Benchmark Points

For collider analysis we choose three representative benchmark points such that the decays $H_1^{++} \rightarrow H_2^{++}h$ and $H_1^{++} \rightarrow H_2^+W^+$ are kinematically allowed. Also, the mass splitting ΔM between the doubly and singly charged higgses for each of the triplet scalar fields are consistent ($\Delta M \leq 50$ GeV) [50, 51] with the ρ parameter constraint. All three benchmark points are also consistent with the observed Higgs signal strength. In Table 1 we show thirteen model parameters as defined in the scalar potential in Eq. 12) that determine the benchmark points. One can see from the table that the values of some of the parameters are kept fixed while others (B, D, E, F, c) have been varied, since the scalar masses are strongly dependent on the latter². Table 2 lists the corresponding values of neutral, singly charged and doubly charged scalar masses. The corresponding mixing angles in different sectors are shown in Table 3. The mixing angles between the doubly charged higgses, singly charged scalars, and CP even neutral scalars (same as CP odd scalars) are denoted by α, β and γ respectively.

| | a | B | D | E | H | F | c | g | g' | t_1 | t_2 | w_1 (in GeV) | w_2 (in GeV) |
|-----|--------|--|--|--|--|--|------|------|------|-------|-------|-------------------|-------------------|
| BP1 | -15625 | $\begin{pmatrix} 41012.0 & -31980.0 \\ -31980.0 & 21182.4 \end{pmatrix}$ | $\begin{pmatrix} 4.00 & 3.56 \\ 3.56 & 4.00 \end{pmatrix}$ | $\begin{pmatrix} 2.64 & 2.80 \\ 2.80 & 2.64 \end{pmatrix}$ | $\begin{pmatrix} 1.00 & 1.00 \\ 1.00 & 1.00 \end{pmatrix}$ | $\begin{pmatrix} 4.00 & 2.00 \\ 2.00 & 4.00 \end{pmatrix}$ | 0.26 | 0.90 | 0.90 | -1 | -2 | 1.09 | 1.32 |
| BP2 | -15625 | $\begin{pmatrix} 43012.0 & -31998.0 \\ -31998.0 & 23182.4 \end{pmatrix}$ | $\begin{pmatrix} 4.00 & 3.40 \\ 3.40 & 4.00 \end{pmatrix}$ | $\begin{pmatrix} 2.54 & 2.80 \\ 2.80 & 2.54 \end{pmatrix}$ | $\begin{pmatrix} 1.00 & 1.00 \\ 1.00 & 1.00 \end{pmatrix}$ | $\begin{pmatrix} 3.50 & 2.00 \\ 2.00 & 3.50 \end{pmatrix}$ | 0.24 | 0.90 | 0.90 | -1 | -2 | 1.09 | 1.32 |
| BP3 | -15625 | $\begin{pmatrix} 41012.0 & -31998.0 \\ -31998.0 & 21182.4 \end{pmatrix}$ | $\begin{pmatrix} 4.00 & 3.60 \\ 3.60 & 4.00 \end{pmatrix}$ | $\begin{pmatrix} 2.74 & 2.80 \\ 2.80 & 2.74 \end{pmatrix}$ | $\begin{pmatrix} 1.00 & 1.00 \\ 1.00 & 1.00 \end{pmatrix}$ | $\begin{pmatrix} 3.00 & 2.00 \\ 2.00 & 3.00 \end{pmatrix}$ | 0.25 | 0.90 | 0.90 | -1 | -2 | 1.09 | 1.32 |

Table 1: *Parameters for all benchmark points.*

² We have kept the triplet vevs fixed at ~ 1 GeV throughout our analysis to allow maximum mixing between the doublet and the triplet scalars as permitted by ρ parameter constraint [24] for all the three benchmark points noted in Table 1. In principle, one can reduce the vevs up to 10^{-4} GeV [25–27] and that will not change the decay modes of the non-standard scalars.

| | $m_{H_1^{\pm\pm}}$ (in GeV) | $m_{H_2^{\pm\pm}}$ (in GeV) | $m_{H_1^\pm}$ (in GeV) | $m_{H_2^\pm}$ (in GeV) | m_{H_1}/m_{A_1} (in GeV) | m_{H_2}/m_{A_2} (in GeV) | $\mu_{\gamma\gamma}$ |
|-----|--------------------------------|--------------------------------|---------------------------|---------------------------|-------------------------------|-------------------------------|----------------------|
| BP1 | 416.37 | 216.13 | 402.13 | 215.87 | 276.56 | 161.48 | 1.20 |
| BP2 | 474.20 | 240.09 | 450.80 | 239.40 | 229.60 | 167.60 | 1.15 |
| BP3 | 490.39 | 365.26 | 483.68 | 310.39 | 328.30 | 272.23 | 1.07 |

Table 2: Masses for different non-standard scalars and the corresponding SM Higgs signal strength within 2σ limit of the current value $1.02^{+0.18}_{-0.19}$ [76].

| | $\sin \alpha$ | $\sin \beta$ | $\sin \gamma$ |
|-----|---------------|--------------|---------------|
| BP1 | 0.76 | 0.63 | 0.55 |
| BP2 | 0.66 | 0.65 | 0.35 |
| BP3 | 0.73 | 0.70 | 0.61 |

Table 3: Mixing angles between for the doubly charged (α), singly charged (β) and CP-even(CP-odd) scalars(γ).

Even after fixing fixed all model parameters in Table 1, the Yukawa coupling matrices $h^{(1)}$ and $h^{(2)}$ still remain indeterminate (Eq. 28). We fix the matrix $h^{(2)}$ by choosing one suitable value for all elements of the μ - τ block and keeping the rest of the elements one order smaller. It is emphasized that this *ad hoc* convention does not affect the generality of our results. One may thus write

$$\begin{aligned}
h_{ij}^{(1)} &= \begin{pmatrix} 4.52 \times 10^{-12} & 1.02 \times 10^{-11} & 3.47 \times 10^{-12} \\ 1.02 \times 10^{-11} & 2.12 \times 10^{-11} & 1.90 \times 10^{-11} \\ 3.47 \times 10^{-12} & 1.90 \times 10^{-11} & 3.68 \times 10^{-11} \end{pmatrix}, \\
h_{ij}^{(2)} &= \begin{pmatrix} 1.0 \times 10^{-12} & 1.0 \times 10^{-12} & 1.0 \times 10^{-12} \\ 1.0 \times 10^{-12} & 1.0 \times 10^{-11} & 1.0 \times 10^{-11} \\ 1.0 \times 10^{-12} & 1.0 \times 10^{-11} & 1.0 \times 10^{-11} \end{pmatrix}.
\end{aligned}$$

IV.2 Collider search at the LHC

We finally turn to signals of this scenario at the high energy high luminosity (HE-HL) run of the LHC. There are several production and decay chains that lead to our chosen final state Eq.(35) ³

$$pp \rightarrow H_1^{++} H_1^{--} \rightarrow (H_2^{++} h) + (H_2^{--} h) \rightarrow (W^+ W^+ h) + (W^- W^- h) \rightarrow 2(\ell^\pm \ell^\pm) + 4b + \cancel{E}_T \quad (36a)$$

$$pp \rightarrow H_1^{++} H_1^{--} \rightarrow (H_2^+ W^+) + (H_2^- W^-) \rightarrow (W^+ W^+ h) + (W^- W^- h) \rightarrow 2(\ell^\pm \ell^\pm) + 4b + \cancel{E}_T \quad (36b)$$

$$pp \rightarrow H_1^{++} H_1^{--} \rightarrow (H_2^+ W^+) + (H_2^- h) \rightarrow (W^+ W^+ h) + (W^- W^- h) \rightarrow 2(\ell^\pm \ell^\pm) + 4b + \cancel{E}_T \quad (36c)$$

$$pp \rightarrow H_1^{++} H_1^{--} \rightarrow (H_2^{++} h) + (H_2^- W^-) \rightarrow (W^+ W^+ h) + (W^- W^- h) \rightarrow 2(\ell^\pm \ell^\pm) + 4b + \cancel{E}_T. \quad (36d)$$

³ For benchmark points BP1 and BP3, the main contribution comes from 36b as $\text{BR}(H_1^{++} \rightarrow H_2^+ W^+) \simeq 99\%$. However, situation is different for BP2, where, $\text{BR}(H_1^{++} \rightarrow H_2^{++} h) \simeq 23\%$, making all the four production and decay modes significant.

It should be noted that $Br(H_2^+ \rightarrow W^+Z)$ and $Br(H_2^+ \rightarrow t\bar{b})$ could give rise to the same final state. However, $Br(H_2^+ \rightarrow W^+h)$ is 99.99%, 97.60% and 99.5% for BP1, BP2 and BP3 respectively. The W^+h mode dominates over W^+Z and $t\bar{b}$ as the W^+h channel receives a single-fold suppression due to doublet-triplet mixings while the two remaining channels (W^+Z , $t\bar{b}$) have two-fold suppression, namely, that from mixing as well as by the small triplet vev which explicitly enters into the couplings. There is a further cancellation between the two above mentioned effects for the W^+Z and $t\bar{b}$ channels making the branching fraction negligible for these two decay modes.

We calculate the event rates in Madgraph5(v2.4.3) [77] with the appropriate Feynman rules obtained via `FeynRules` [78]. The signal as well as all the relevant standard model background events are calculated at the lowest order (LO) with `CTEQ6L` [79] parton distribution functions, setting the renormalization and factorization scales at M_Z . They are subsequently multiplied by the next-to-leading order (NLO) K-factors for the signal and the SM background processes, taken as 1.25 [80] and 1.3 [81–83] respectively. For the showering and hadronization of both the signal and the SM background events we use the `Pythia`(v6.4) [84], and the detector simulation is done in `Delphes`(v3) [85], where jets are constructed using the anti- K_T algorithm [86]. The cut-based analyses are done using the `MadAnalysis5` [87]. The production of $t\bar{t}Z$, $t\bar{t}W^\pm$ and $t\bar{t}h$ constitute the dominant SM background for our signal. While generating events, we select jets and leptons (electron and muon) using the following kinematical acceptance cuts :

$$\Delta R_{jj} > 0.6, \quad \Delta R_{\ell\ell} > 0.4, \quad \Delta R_{j\ell} > 0.7, \quad (37a)$$

$$\Delta R_{bj} > 0.7, \quad \Delta R_{b\ell} > 0.2, \quad (37b)$$

$$p_{T_{\min}}^j > 20 \text{ GeV}, \quad |\eta_j| < 5, \quad (37c)$$

$$p_{T_{\min}}^\ell > 10 \text{ GeV}, \quad |\eta_\ell| < 2.5, \quad (37d)$$

The presence of four b-jets in the signal makes b-tagging an important issue. For this we comply with the efficiency formula proposed by the ATLAS collaboration [88] for both the signal and background processes as follows:

$$\epsilon_b = \begin{cases} 0 & p_T^b \leq 30 \text{ GeV} \\ 0.6 & 30 \text{ GeV} < p_T^b < 50 \text{ GeV} \\ 0.75 & 50 \text{ GeV} < p_T^b < 400 \text{ GeV} \\ 0.5 & p_T^b > 400 \text{ GeV} . \end{cases} \quad (38)$$

In addition, a mistagging probability of 10% (1%) for charm-jets (light-quark and gluon jets) as a b -jet has been taken into account. For lepton isolation, we abide by the criteria defined in Ref. [89] where the electrons are isolated with the `Tight` criterion defined in Ref. [90] and the muons are isolated using the `Medium` criterion defined in reference [91].

One point worth mentioning at this point is that we consider the all inclusive decay channels for both the signal and background event generation, not only the leptonic decay of the SM W^\pm boson. This is true for all the subsequent analyses. Before reporting the results in detail,

let us examine some kinematic distributions relevant for the analysis, starting with transverse momenta (p_T) of the two leading leptons as depicted in Figure 1 for BP1. The signal and background distributions are shown in blue and red respectively. In the signal events, these leptons originate from the decay of the W boson, while for the SM background processes, they come from the decay of W^\pm or Z -bosons. From the shape of the p_T distribution one can see that it is evidently difficult to impose any selection cut on the p_T of these two leading leptons to distinguish the signal from the SM backgrounds. This general feature is also found for other two benchmark points. Hence, we only put the basic acceptance cut on the p_T of the leptons, $p_T > 10$ GeV.

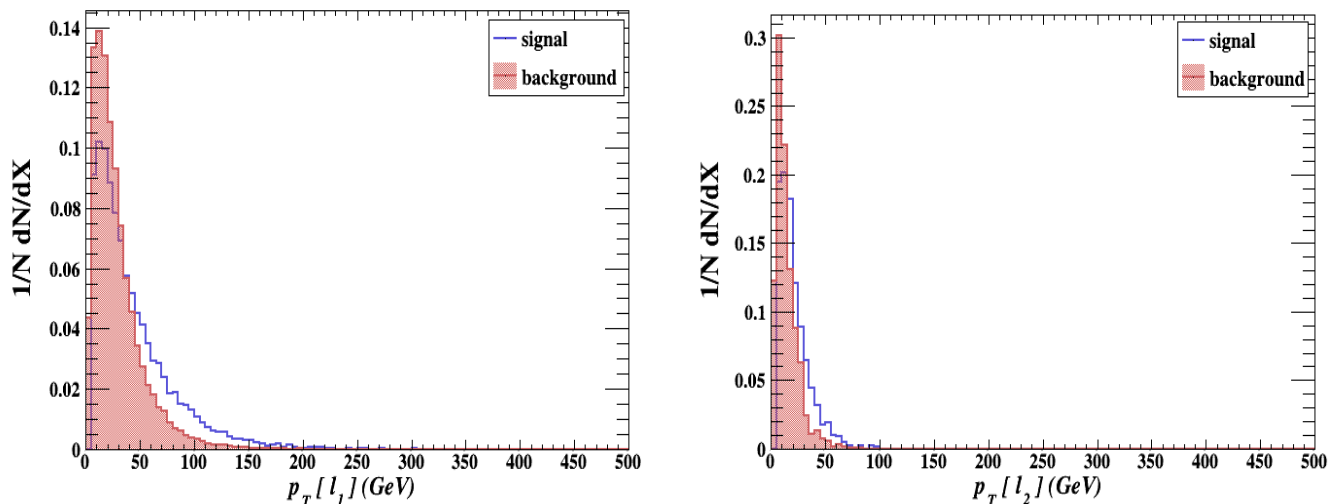


Figure 1: *Transverse momentum (p_T) distribution (normalized) of the leading and subleading leptons for the benchmark BP1.*

In Figure 2 we show the P_T distributions of four b -jets for both signal and background events. In the signal events, they come from decays of two SM-like scalars each of which is produced via either from $H_1^{\pm\pm} \rightarrow H_2^{\pm\pm}h \rightarrow W^\pm W^\pm h$ or from $H_1^{\pm\pm} \rightarrow H_2^\pm W^\pm \rightarrow W^\pm W^\pm h$. On the other hand, the background b -jets have their sources mostly in $t\bar{t}h$, $t\bar{t}W^\pm$ and $t\bar{t}Z$. In the case of $t\bar{t}W^\pm$ production, two b -jets come from the top quarks, while a pair of light quark jets may fake as b -jets. The leading b -jet of our signal events is found to be harder than that of those in the background. Thus we demand the leading b -jet to have $p_T(j_1) > 80$ GeV, and p_T of the subsequent 3 b -jets to be $p_T(j_2) > 60$ GeV, $p_T(j_3) > 30$ GeV and $p_T(j_4) > 20$ GeV.

The normalized distribution of the missing transverse energy (\cancel{E}_T) are in the left panel of Figure 3. One should note that the \cancel{E}_T for both signal and backgrounds is due to either neutrinos or the missmeasurement of the jet and lepton momenta. Consequently, the shape of the distributions for both the signal and the background look very similar. The small rightward shift of the peak of the signal distribution can be attributed to fact that W^\pm are boosted as they are produced from the decays of much heavier parent scalars. Hence, we find that a moderate requirement of $\cancel{E}_T > 30$ GeV is sufficient to improve the signal to background ratio.

The right panel of Figure 3 shows the normalized distribution of angular separation $\Delta R(\ell^\pm \ell^\pm)$

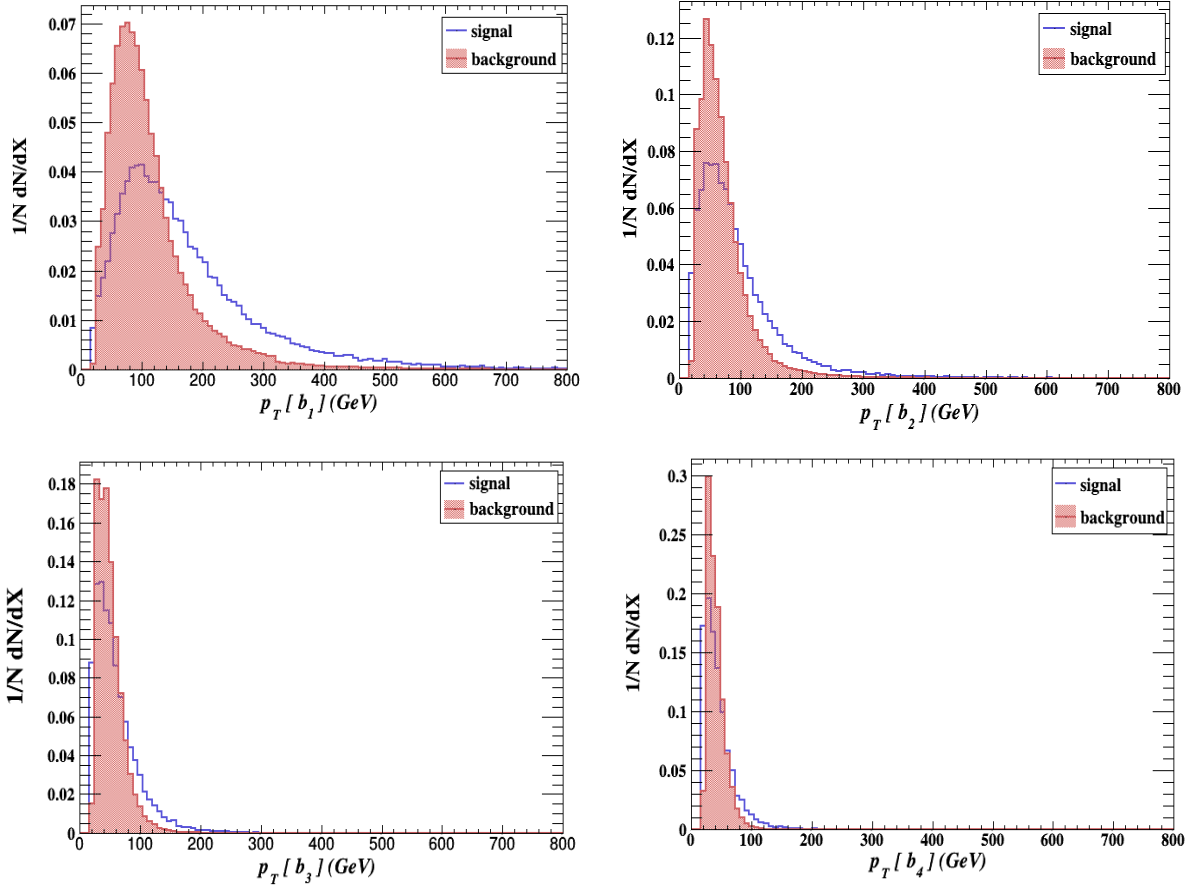


Figure 2: *Transverse momentum (p_T) distribution (normalized) of the four leading b jets for the final state $2\ell^\pm\ell^\pm + 4b + \cancel{E}_T$ for the benchmark BP1.*

between two same-sign leptons for both the signal and the background events. For our signal events, both leptons come from same-sign W^\pm which are produced from the decay of heavy doubly charged scalar with non-zero transverse momenta. The P_T of the heavy doubly charged scalar forces its decay products (W -pair) to appear with relatively small ΔR . The resultant effect of these two is finally displayed by the two same-sign leptons that also appear with small opening angle. For the SM background, on the other hand, they come from W^\pm/Z bosons radiated from top/anti-top quarks, and can have wider separations. An upper cut on $\Delta R(\ell_1^\pm\ell_2^\pm) < 1.5$ thus enhances our signal-to-background ratio.

The cuts are summarised below, in the order in which they are imposed:

- (C-1): We want the leading b -jet to have $p_T(b_1) > 80$ GeV. This is motivated by the top-left panel of Figure 2 and it immediately reduces the SM background arising from $t\bar{t}V$, $V \equiv W^\pm, Z$ processes by almost 50%.
- (C-2): Given the fact that the second leading b -jet for the signal is not very hard, we demand that $p_T(b_2) > 60$ GeV. This cut also enhances the signal to background ratio to

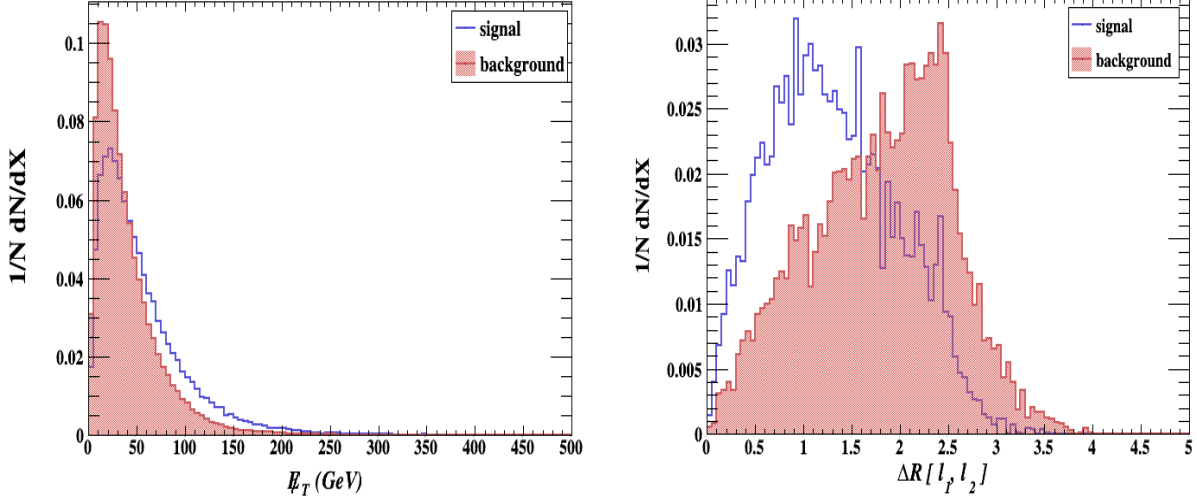


Figure 3: *The normalized missing transverse energy distribution (left panel) E_T and $\Delta R(\ell_1^\pm \ell_2^\pm)$ distribution (normalized) (right panel) between the two same-sign leptons for the benchmark BP1.*

a reasonable extent.

- (C-3): $p_T(b_3)$ is chosen to be > 30 GeV.
- (C-4): It is evident from the bottom-right panel of Figure 2 that the fourth b jet is very soft. So, the choice of $p_T(b_4) > 20$ GeV ensures the presence of four b jets in the signal.
- (C-5): We select two same sign leptons with $p_T > 10$ GeV.
- (C-6): We apply a veto on any oppositely charged lepton with $p_T(\ell) > 10$ GeV.
- (C-7): $E_T > 30$ GeV is imposed. This also takes care of fake E_T .
- (C-8): The most effective cut to reduce the SM backgrounds is the angular separation between the same sign dileptons. The requirement of $\Delta R(\ell_1^\pm \ell_2^\pm) < 1.5$ considerably improves the signal to noise ratio.

With these cuts imposed, we obtain the statistical significance of the signal HE-HL LHC with $\sqrt{s} = 14$ TeV and also present some tentative predictions for the proposed FCC-hh with $\sqrt{s} = 100$ TeV.

IV.2.1 Collider search at the LHC at $\sqrt{s} = 14$ TeV

Table 4 contains the cut flow for $\sqrt{s} = 14$ TeV. The statistical significance is given by

$$\mathcal{S} = \sqrt{2 \times [(n_s + n_b) \ln(1 + \frac{n_s}{n_b}) - n_s]}, \quad (39)$$

where $n_s(n_b)$ denotes the number of signal (background) events after implementing all the cuts at a specific luminosity. The signal significance can be seen for three benchmark points, assuming an integrated luminosity \mathcal{L}_{int} of 3 ab^{-1} . We obtain the highest statistical significance $\mathcal{S} = 5.80$ for BP1, which corresponds to $m_{H_1^{\pm\pm}} = 416.37 \text{ GeV}$ and $m_{H_2^{\pm\pm}} = 216.13 \text{ GeV}$ respectively. For the other two benchmark points with relatively heavier scalar masses, the significances are 3.03σ and 1.84σ respectively, which may be treated as the evidence of the two-triplet scenario.

| SM-background | Production Cross section (fb) | Effective cross section (fb) after the cut | | | | | | | | |
|---------------------|-------------------------------|---|--------|--------|-------|--------|--------|--------|--------|--|
| | | C1-1 | C1-2 | C1-3 | C1-4 | C1-5 | C1-6 | C1-7 | C1-8 | |
| $tt + W^{\pm}$ | 517.4 | 280.59 | 96.81 | 11.27 | 0.51 | 0.0028 | 0.0023 | 0.002 | 0.0001 | |
| $tt + Z$ | 917.8 | 436.06 | 214.72 | 56.28 | 10.37 | 0.009 | 0.0052 | 0.004 | 0.0004 | |
| $tt + h$ | 622.7 | 535.21 | 242.88 | 121.93 | 31.36 | 0.0026 | 0.0016 | 0.001 | 0.0001 | |
| Total SM Background | 2058 | 1251.86 | 554.41 | 189.48 | 42.24 | 0.0144 | 0.0091 | 0.007 | 0.0006 | |
| Signal | Production Cross section (fb) | Effective cross section (fb) for signal after the cut | | | | | | | | Significance reach at $\mathcal{L}_{\text{int}} = 3 \text{ ab}^{-1}$ |
| BP1 | 4.41 | 3.59 | 2.44 | 1.56 | 0.66 | 0.011 | 0.009 | 0.008 | 0.0042 | |
| BP2 | 2.08 | 1.71 | 1.16 | 0.74 | 0.32 | 0.0051 | 0.0044 | 0.0035 | 0.0018 | 3.03 |
| BP3 | 1.05 | 0.86 | 0.58 | 0.37 | 0.16 | 0.0025 | 0.0019 | 0.0016 | 0.0010 | 1.84 |

Table 4: *Effective cross section obtained after each cut for both signal ($2(\ell^{\pm}\ell^{\pm}) + 4b + \cancel{E}_T$) and background and the respective significance reach at 3 ab^{-1} integrated luminosity at 14 TeV LHC*

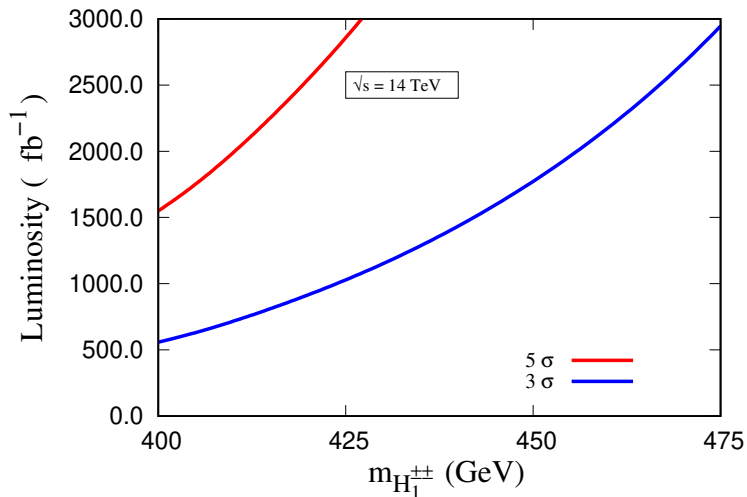


Figure 4: *Variation of the integrated luminosity (\mathcal{L}_{int}) as a function of the doubly charged scalar mass($m_{H_1^{\pm\pm}}$) at the 14 TeV LHC. The red and blue lines correspond to the \mathcal{L}_{int} required for the 5σ discovery and 3σ evidence respectively for the signal studied.*

In Figure 4 we present the doubly charged scalar($H_1^{\pm\pm}$) mass and the integrated luminosity(\mathcal{L}_{int}) required to reach 5σ (red solid line) and 3σ (blue solid line) significance with 14 TeV. It is evident

from this Figure that ‘discovery’ is not possible beyond $m_{H_1^{\pm\pm}} \sim 430$ GeV even with 3ab^{-1} . However, one can probe the doubly charged scalar mass up to 475 GeV at 3σ level.

Figure 5 shows the variation of \mathcal{S} in the $m_{H_1^{\pm\pm}} - m_{H_2^{\pm\pm}}$ plane. \mathcal{S} drops from 7σ to 2σ as mass of $H_1^{\pm\pm}(H_2^{\pm\pm})$ is increased from 400(206) GeV to 490(370) GeV due to phase space suppression. It is worth mentioning here that, for the single-triplet case with $w \sim 1$ GeV, doubly charged scalar masses up to 300 GeV can be explored at the 5σ level at the LHC with an integrated luminosity of 3 ab^{-1} [41].

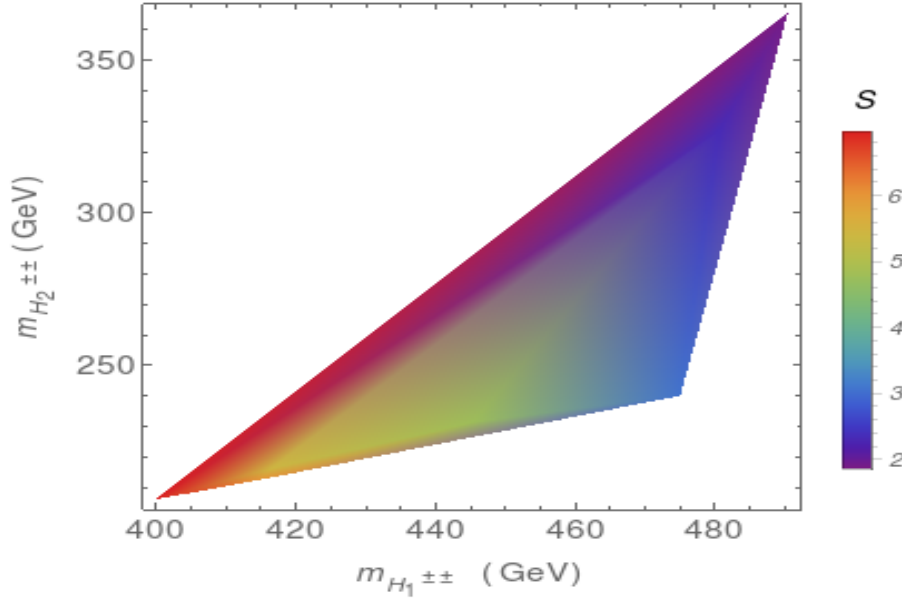


Figure 5: *Signal significance (\mathcal{S}) in the $m_{H_1^{\pm\pm}} - m_{H_2^{\pm\pm}}$ plane, shown with continuously varying colour codes, for 3 ab^{-1} integrated luminosity at 14 TeV .*

IV.2.2 Search at $\sqrt{s} = 100$ TeV FCC-hh collider

We next make a tentative estimate of the potential of the proposed 100 TeV FCC-hh to investigate the two triplet scalar scenario. In our numerical analysis, we apply the set of selection cuts as those used for the 14 TeV LHC. Since the production mode of our signal processes are electroweak processes, the NLO K-factors, too, are taken to be the same, an assumption justifiable in the light of [92]. Table 5 summarises the effect of different selection cuts on the signal and the SM backgrounds for all the three benchmark points. At this energy, all of them can be probed with $\mathcal{S} \geq 5\sigma$ at 3ab^{-1} . A comparison with the 14 TeV LHC shows that, while a 5σ reach with (3ab^{-1}) is possible only for BP1, a distinct improvement is foreseen for the FCC-hh. This is reflected in Figure 6 which shows that one can probe doubly charged Higgs masses up to 495(540) GeV at the $5\sigma(3\sigma)$ significance level.

| SM-background | Production Cross section (fb) | Effective cross section (fb) after the cut | | | | | | | | |
|---------------------|-------------------------------|---|--------------------|--------------------|--------------------|-------|-------|-------|-------|--|
| | | C2-1 | C2-2 | C2-3 | C2-4 | C2-5 | C2-6 | C2-7 | C2-8 | |
| $t\bar{t} + W^\pm$ | 2.07×10^4 | 6.27×10^3 | 1.18×10^3 | 1.84×10^2 | 10.73 | 0.10 | 0.081 | 0.040 | 0.004 | |
| $t\bar{t} + Z$ | 6.41×10^4 | 3.10×10^4 | 1.12×10^4 | 2.77×10^3 | 55.09 | 0.13 | 0.12 | 0.116 | 0.009 | |
| $t\bar{t} + h$ | 3.80×10^4 | 2.46×10^4 | 1.24×10^4 | 5.68×10^3 | 1.51×10^3 | 0.23 | 0.22 | 0.21 | 0.015 | |
| Total SM Background | 1.11×10^5 | 6.19×10^4 | 2.48×10^4 | 8.63×10^3 | 1.57×10^3 | 0.46 | 0.42 | 0.366 | 0.028 | |
| Signal | Production Cross section (fb) | Effective cross section (fb) for signal after the cut | | | | | | | | Significance reach at $\mathcal{L}_{\text{int}} = 3 \text{ ab}^{-1}$ |
| BP1 | 125.0 | 83.59 | 51.08 | 30.29 | 12.35 | 0.142 | 0.122 | 0.121 | 0.072 | 18.21 |
| BP2 | 68.08 | 45.90 | 27.99 | 16.60 | 6.67 | 0.077 | 0.066 | 0.065 | 0.039 | 10.80 |
| BP3 | 28.81 | 19.35 | 11.83 | 7.02 | 2.88 | 0.034 | 0.029 | 0.028 | 0.020 | 5.94 |

Table 5: *Effective cross section obtained after each cut for both signal ($2(\ell^\pm\ell^\pm) + 4b + \cancel{E}_T$) and background and the respective significance reach at 3 ab^{-1} integrated luminosity at 100 TeV pp collider*

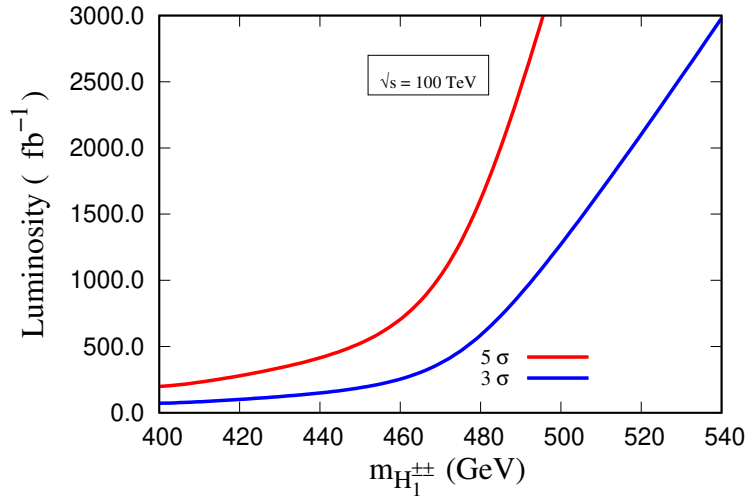


Figure 6: *Same as in Figure 4 for the 100 TeV FCC-hh.*

The signal topology studied in this work strongly depends on $m_{H_1^{\pm\pm}}$, $m_{H_2^{\pm\pm}}$ and their mass splitting. This is accentuated in Figure 7 where we show the dependence of the signal significance on these two masses. using colour-codes significance regions once more.

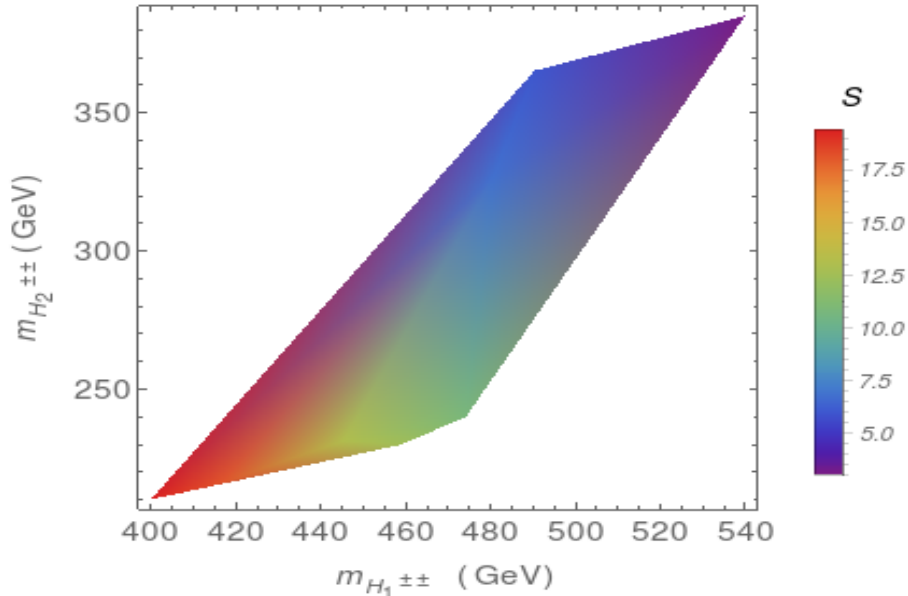


Figure 7: Same as in Figure 5 for the 100 TeV FCC-hh.

V Conclusion

We have extended the Type-II seesaw model with an extra $SU(2)_L$ complex triplet scalar and allow a small mixing of the triplets with the SM Higgs doublet as required by electroweak precision measurements. After EWSB, one has a rather rich scalar spectrum including two each of doubly and singly charged scalars. A collider signal distinctly reflecting the presence of two triplets is identified in the form of $2\ell^\pm\ell^\pm + 4b + \cancel{E}_T$. This channel can arise both from $H_1^{\pm\pm} \rightarrow H_2^{\pm\pm}h$ and $H_1^{\pm\pm} \rightarrow H_2^\pm W^\pm$ following the characteristic decay modes in the case where the Yukawa couplings are too small (large triplet vev) to trigger the dominant same-sign-dilepton channels. Three benchmark points, consistent with all phenomenological constraints, have been used as illustration. We have estimated the potential at high luminosity LHC and a high energy pp collider 100 TeV in identifying this signal.

We conclude after a cut-based analysis that the 5σ discovery reach is possible with 3 ab^{-1} luminosity at 14 TeV LHC for the mass of the heavier doubly charged scalar up to about 430 GeV. For the proposed FCC-hh collider operating at $\sqrt{s} = 100 \text{ TeV}$, this reach can be extended up to 495 GeV. Though we have not taken into account some experimental issues such as jet faking leptons, lepton charge misidentification and photon conversions into lepton pairs, these effects are unlikely to affect the predictions qualitatively. Therefore, with appropriate refinement, our prediction should help in probing this scenario which is relevant in framing predictive models for neutrino masses and mixing.

VI Acknowledgement

NG would like to acknowledge the Council of Scientific and Industrial Research (CSIR), Government of India for financial support. BM acknowledges financial support from the Department of Atomic Energy, Government of India, for the Regional Centre for Accelerator-based Particle Physics (RECAPP), Harish-Chandra Research Institute. DKG and NG thank RECAPP for hospitality while this work was being carried out. BM would like to thank Indian Association for the Cultivation of Science for hospitality during the concluding part of the project.

References

- [1] ATLAS collaboration, G. Aad et al., *Observation of a new particle in the search for the Standard Model Higgs boson with the ATLAS detector at the LHC*, *Phys. Lett.* **B716** (2012) 1–29, [[1207.7214](#)].
- [2] CMS collaboration, S. Chatrchyan et al., *Observation of a new boson at a mass of 125 GeV with the CMS experiment at the LHC*, *Phys. Lett.* **B716** (2012) 30–61, [[1207.7235](#)].
- [3] C. W. Walter, *The Super-Kamiokande Experiment*, [0802.1041](#).
- [4] M. C. Gonzalez-Garcia and M. Maltoni, *Phenomenology with Massive Neutrinos*, *Phys. Rept.* **460** (2008) 1–129, [[0704.1800](#)].
- [5] R. N. Mohapatra and A. Y. Smirnov, *Neutrino Mass and New Physics*, *Ann. Rev. Nucl. Part. Sci.* **56** (2006) 569–628, [[hep-ph/0603118](#)].
- [6] P. Minkowski, $\mu \rightarrow e\gamma$ at a Rate of One Out of 10^9 Muon Decays?, *Phys. Lett.* **67B** (1977) 421–428.
- [7] T. Yanagida, *HORIZONTAL SYMMETRY AND MASSES OF NEUTRINOS*, *Conf. Proc.* **C7902131** (1979) 95–99.
- [8] R. N. Mohapatra and G. Senjanovic, *Neutrino Mass and Spontaneous Parity Violation*, *Phys. Rev. Lett.* **44** (1980) 912.
- [9] J. Schechter and J. W. F. Valle, *Neutrino Masses in $SU(2) \times U(1)$ Theories*, *Phys. Rev.* **D22** (1980) 2227.
- [10] M. Magg and C. Wetterich, *Neutrino Mass Problem and Gauge Hierarchy*, *Phys. Lett.* **94B** (1980) 61–64.
- [11] T. P. Cheng and L.-F. Li, *Neutrino Masses, Mixings and Oscillations in $SU(2) \times U(1)$ Models of Electroweak Interactions*, *Phys. Rev.* **D22** (1980) 2860.
- [12] G. Lazarides, Q. Shafi and C. Wetterich, *Proton Lifetime and Fermion Masses in an $SO(10)$ Model*, *Nucl. Phys.* **B181** (1981) 287–300.

- [13] R. N. Mohapatra and G. Senjanovic, *Neutrino Masses and Mixings in Gauge Models with Spontaneous Parity Violation*, *Phys. Rev.* **D23** (1981) 165.
- [14] R. Foot, H. Lew, X. G. He and G. C. Joshi, *Seesaw Neutrino Masses Induced by a Triplet of Leptons*, *Z. Phys.* **C44** (1989) 441.
- [15] R. Franceschini, T. Hambye and A. Strumia, *Type-III see-saw at LHC*, *Phys. Rev.* **D78** (2008) 033002, [[0805.1613](#)].
- [16] F. del Aguila and J. A. Aguilar-Saavedra, *Distinguishing seesaw models at LHC with multi-lepton signals*, *Nucl. Phys.* **B813** (2009) 22–90, [[0808.2468](#)].
- [17] A. Arhrib, B. Bajc, D. K. Ghosh, T. Han, G.-Y. Huang, I. Puljak et al., *Collider Signatures for Heavy Lepton Triplet in Type I+III Seesaw*, *Phys. Rev.* **D82** (2010) 053004, [[0904.2390](#)].
- [18] A. G. Akeroyd and M. Aoki, *Single and pair production of doubly charged Higgs bosons at hadron colliders*, *Phys. Rev.* **D72** (2005) 035011, [[hep-ph/0506176](#)].
- [19] A. G. Akeroyd and C.-W. Chiang, *Doubly charged Higgs bosons and three-lepton signatures in the Higgs Triplet Model*, *Phys. Rev.* **D80** (2009) 113010, [[0909.4419](#)].
- [20] A. G. Akeroyd and C.-W. Chiang, *Phenomenology of Large Mixing for the CP-even Neutral Scalars of the Higgs Triplet Model*, *Phys. Rev.* **D81** (2010) 115007, [[1003.3724](#)].
- [21] A. G. Akeroyd and H. Sugiyama, *Production of doubly charged scalars from the decay of singly charged scalars in the Higgs Triplet Model*, *Phys. Rev.* **D84** (2011) 035010, [[1105.2209](#)].
- [22] M. Lindner, M. Platscher and F. S. Queiroz, *A Call for New Physics : The Muon Anomalous Magnetic Moment and Lepton Flavor Violation*, *Phys. Rept.* **731** (2018) 1–82, [[1610.06587](#)].
- [23] A. Arhrib, R. Benbrik, M. Chabab, G. Moultaqa, M. C. Peyranere, L. Rahili et al., *The Higgs Potential in the Type II Seesaw Model*, *Phys. Rev.* **D84** (2011) 095005, [[1105.1925](#)].
- [24] M. Aoki, S. Kanemura, M. Kikuchi and K. Yagyu, *Radiative corrections to the Higgs boson couplings in the triplet model*, *Phys. Rev.* **D87** (2013) 015012, [[1211.6029](#)].
- [25] P. Fileviez Perez, T. Han, G.-y. Huang, T. Li and K. Wang, *Neutrino Masses and the CERN LHC: Testing Type II Seesaw*, *Phys. Rev.* **D78** (2008) 015018, [[0805.3536](#)].
- [26] A. Melfo, M. Nemevsek, F. Nesti, G. Senjanovic and Y. Zhang, *Type II Seesaw at LHC: The Roadmap*, *Phys. Rev.* **D85** (2012) 055018, [[1108.4416](#)].
- [27] M. Aoki, S. Kanemura and K. Yagyu, *Testing the Higgs triplet model with the mass difference at the LHC*, *Phys. Rev.* **D85** (2012) 055007, [[1110.4625](#)].

- [28] ATLAS collaboration, T. A. collaboration, *Search for doubly-charged Higgs boson production in multi-lepton final states with the ATLAS detector using proton-proton collisions at $\sqrt{s} = 13$ TeV*, ATLAS-CONF-2017-053.
- [29] T. Han, B. Mukhopadhyaya, Z. Si and K. Wang, *Pair production of doubly-charged scalars: Neutrino mass constraints and signals at the LHC*, *Phys. Rev.* **D76** (2007) 075013, [[0706.0441](#)].
- [30] S. Chakrabarti, D. Choudhury, R. M. Godbole and B. Mukhopadhyaya, *Observing doubly charged Higgs bosons in photon-photon collisions*, *Phys. Lett.* **B434** (1998) 347–353, [[hep-ph/9804297](#)].
- [31] K. Cheung and D. K. Ghosh, *Triplet Higgs boson at hadron colliders*, *JHEP* **11** (2002) 048, [[hep-ph/0208254](#)].
- [32] C.-W. Chiang, T. Nomura and K. Tsumura, *Search for doubly charged Higgs bosons using the same-sign diboson mode at the LHC*, *Phys. Rev.* **D85** (2012) 095023, [[1202.2014](#)].
- [33] S. Kanemura, K. Yagyu and H. Yokoya, *First constraint on the mass of doubly-charged Higgs bosons in the same-sign diboson decay scenario at the LHC*, *Phys. Lett.* **B726** (2013) 316–319, [[1305.2383](#)].
- [34] Z. Kang, J. Li, T. Li, Y. Liu and G.-Z. Ning, *Light Doubly Charged Higgs Boson via the WW^* Channel at LHC*, *Eur. Phys. J.* **C75** (2015) 574, [[1404.5207](#)].
- [35] S. Kanemura, M. Kikuchi, K. Yagyu and H. Yokoya, *Bounds on the mass of doubly-charged Higgs bosons in the same-sign diboson decay scenario*, *Phys. Rev.* **D90** (2014) 115018, [[1407.6547](#)].
- [36] S. Kanemura, M. Kikuchi, H. Yokoya and K. Yagyu, *LHC Run-I constraint on the mass of doubly charged Higgs bosons in the same-sign diboson decay scenario*, *PTEP* **2015** (2015) 051B02, [[1412.7603](#)].
- [37] C.-H. Chen and T. Nomura, *Search for $\delta^{\pm\pm}$ with new decay patterns at the LHC*, *Phys. Rev.* **D91** (2015) 035023, [[1411.6412](#)].
- [38] Z.-L. Han, R. Ding and Y. Liao, *LHC Phenomenology of Type II Seesaw: Nondegenerate Case*, *Phys. Rev.* **D91** (2015) 093006, [[1502.05242](#)].
- [39] Z.-L. Han, R. Ding and Y. Liao, *LHC phenomenology of the type II seesaw mechanism: Observability of neutral scalars in the nondegenerate case*, *Phys. Rev.* **D92** (2015) 033014, [[1506.08996](#)].
- [40] M. Mitra, S. Niyogi and M. Spannowsky, *Type-II Seesaw Model and Multilepton Signatures at Hadron Colliders*, *Phys. Rev.* **D95** (2017) 035042, [[1611.09594](#)].
- [41] D. K. Ghosh, N. Ghosh, I. Saha and A. Shaw, *Revisiting the high-scale validity of the type II seesaw model with novel LHC signature*, *Phys. Rev.* **D97** (2018) 115022, [[1711.06062](#)].

- [42] P. S. B. Dev and Y. Zhang, *Displaced vertex signatures of doubly charged scalars in the type-II seesaw and its left-right extensions*, [1808.00943](#).
- [43] W. Grimus, A. S. Joshipura, L. Lavoura and M. Tanimoto, *Symmetry realization of texture zeros*, *Eur. Phys. J.* **C36** (2004) 227–232, [[hep-ph/0405016](#)].
- [44] A. Chaudhuri, W. Grimus and B. Mukhopadhyaya, *Doubly charged scalar decays in a type II seesaw scenario with two Higgs triplets*, *JHEP* **02** (2014) 060, [[1305.5761](#)].
- [45] A. Chaudhuri and B. Mukhopadhyaya, *CP -violating phase in a two Higgs triplet scenario: Some phenomenological implications*, *Phys. Rev.* **D93** (2016) 093003, [[1602.07846](#)].
- [46] T. Golling et al., *Physics at a 100 TeV pp collider: beyond the Standard Model phenomena*, *CERN Yellow Report* (2017) 441–634, [[1606.00947](#)].
- [47] J. Tang et al., *Concept for a Future Super Proton-Proton Collider*, [1507.03224](#).
- [48] N. Arkani-Hamed, T. Han, M. Mangano and L.-T. Wang, *Physics opportunities of a 100 TeV protonproton collider*, *Phys. Rept.* **652** (2016) 1–49, [[1511.06495](#)].
- [49] PARTICLE DATA GROUP collaboration, C. Patrignani et al., *Review of Particle Physics*, *Chin. Phys.* **C40** (2016) 100001.
- [50] E. J. Chun, H. M. Lee and P. Sharma, *Vacuum Stability, Perturbativity, EWPD and Higgs-to-diphoton rate in Type II Seesaw Models*, *JHEP* **11** (2012) 106, [[1209.1303](#)].
- [51] GFITTER GROUP collaboration, M. Baak, J. Cth, J. Haller, A. Hoecker, R. Kogler, K. Mnig et al., *The global electroweak fit at NNLO and prospects for the LHC and ILC*, *Eur. Phys. J.* **C74** (2014) 3046, [[1407.3792](#)].
- [52] P. H. Frampton, S. L. Glashow and D. Marfatia, *Zeroes of the neutrino mass matrix*, *Phys. Lett.* **B536** (2002) 79–82, [[hep-ph/0201008](#)].
- [53] Z.-z. Xing, *Texture zeros and Majorana phases of the neutrino mass matrix*, *Phys. Lett.* **B530** (2002) 159–166, [[hep-ph/0201151](#)].
- [54] Z.-z. Xing, *A Full determination of the neutrino mass spectrum from two zero textures of the neutrino mass matrix*, *Phys. Lett.* **B539** (2002) 85–90, [[hep-ph/0205032](#)].
- [55] M. Honda, S. Kaneko and M. Tanimoto, *Prediction and its stability in neutrino mass matrix with two zeros*, *JHEP* **09** (2003) 028, [[hep-ph/0303227](#)].
- [56] W.-l. Guo and Z.-z. Xing, *Calculable CP violating phases in the minimal seesaw model of leptogenesis and neutrino mixing*, *Phys. Lett.* **B583** (2004) 163–172, [[hep-ph/0310326](#)].
- [57] M. Honda, S. Kaneko and M. Tanimoto, *Seesaw enhancement of bilarge mixing in two zero textures*, *Phys. Lett.* **B593** (2004) 165–174, [[hep-ph/0401059](#)].

- [58] S. Goswami and A. Watanabe, *Minimal Seesaw Textures with Two Heavy Neutrinos*, *Phys. Rev.* **D79** (2009) 033004, [[0807.3438](#)].
- [59] S. Choubey, W. Rodejohann and P. Roy, *Phenomenological consequences of four zero neutrino Yukawa textures*, *Nucl. Phys.* **B808** (2009) 272–291, [[0807.4289](#)].
- [60] S. Goswami, S. Khan and W. Rodejohann, *Minimal Textures in Seesaw Mass Matrices and their low and high Energy Phenomenology*, *Phys. Lett.* **B680** (2009) 255–262, [[0905.2739](#)].
- [61] H. Fritzsch, Z.-z. Xing and S. Zhou, *Two-zero Textures of the Majorana Neutrino Mass Matrix and Current Experimental Tests*, *JHEP* **09** (2011) 083, [[1108.4534](#)].
- [62] M. Ghosh, S. Goswami and S. Gupta, *Two Zero Mass Matrices and Sterile Neutrinos*, *JHEP* **04** (2013) 103, [[1211.0118](#)].
- [63] J. Liao, D. Marfatia and K. Whisnant, *Neutrino seesaw mechanism with texture zeros*, *Nucl. Phys.* **B900** (2015) 449–476, [[1508.07364](#)].
- [64] T. Kitabayashi and M. Yasu, *Formulas for flavor neutrino masses and their application to texture two zeros*, *Phys. Rev.* **D93** (2016) 053012, [[1512.00913](#)].
- [65] J. M. Lamprea and E. Peinado, *Seesaw scale discrete dark matter and two-zero texture Majorana neutrino mass matrices*, *Phys. Rev.* **D94** (2016) 055007, [[1603.02190](#)].
- [66] W. Grimus and L. Lavoura, *On a model with two zeros in the neutrino mass matrix*, *J. Phys.* **G31** (2005) 693–702, [[hep-ph/0412283](#)].
- [67] PARTICLE DATA GROUP collaboration, J. Beringer et al., *Review of Particle Physics (RPP)*, *Phys. Rev.* **D86** (2012) 010001.
- [68] G. L. Fogli, E. Lisi, A. Marrone, D. Montanino, A. Palazzo and A. M. Rotunno, *Global analysis of neutrino masses, mixings and phases: entering the era of leptonic CP violation searches*, *Phys. Rev.* **D86** (2012) 013012, [[1205.5254](#)].
- [69] DAYA BAY collaboration, F. P. An et al., *Observation of electron-antineutrino disappearance at Daya Bay*, *Phys. Rev. Lett.* **108** (2012) 171803, [[1203.1669](#)].
- [70] RENO collaboration, J. K. Ahn et al., *Observation of Reactor Electron Antineutrino Disappearance in the RENO Experiment*, *Phys. Rev. Lett.* **108** (2012) 191802, [[1204.0626](#)].
- [71] F. Arbabifar, S. Bahrami and M. Frank, *Neutral Higgs Bosons in the Higgs Triplet Model with nontrivial mixing*, *Phys. Rev.* **D87** (2013) 015020, [[1211.6797](#)].
- [72] S. Kanemura and K. Yagyu, *Radiative corrections to electroweak parameters in the Higgs triplet model and implication with the recent Higgs boson searches*, *Phys. Rev.* **D85** (2012) 115009, [[1201.6287](#)].

- [73] A. G. Akeroyd and S. Moretti, *Enhancement of H to gamma gamma from doubly charged scalars in the Higgs Triplet Model*, *Phys. Rev.* **D86** (2012) 035015, [[1206.0535](#)].
- [74] P. S. Bhupal Dev, D. K. Ghosh, N. Okada and I. Saha, *125 GeV Higgs Boson and the Type-II Seesaw Model*, *JHEP* **03** (2013) 150, [[1301.3453](#)].
- [75] D. Das and A. Santamaria, *Updated scalar sector constraints in the Higgs triplet model*, *Phys. Rev.* **D94** (2016) 015015, [[1604.08099](#)].
- [76] CMS collaboration, A. M. Sirunyan et al., *Measurements of Higgs boson properties in the diphoton decay channel in proton-proton collisions at $\sqrt{s} = 13$ TeV*, [1804.02716](#).
- [77] J. Alwall, R. Frederix, S. Frixione, V. Hirschi, F. Maltoni, O. Mattelaer et al., *The automated computation of tree-level and next-to-leading order differential cross sections, and their matching to parton shower simulations*, *JHEP* **07** (2014) 079, [[1405.0301](#)].
- [78] A. Alloul, N. D. Christensen, C. Degrande, C. Duhr and B. Fuks, *FeynRules 2.0 - A complete toolbox for tree-level phenomenology*, *Comput. Phys. Commun.* **185** (2014) 2250–2300, [[1310.1921](#)].
- [79] J. Pumplin, D. R. Stump, J. Huston, H. L. Lai, P. M. Nadolsky and W. K. Tung, *New generation of parton distributions with uncertainties from global QCD analysis*, *JHEP* **07** (2002) 012, [[hep-ph/0201195](#)].
- [80] ATLAS collaboration, T. A. collaboration, *Search for doubly-charged Higgs bosons in same-charge electron pair final states using proton-proton collisions at $\sqrt{s} = 13$ TeV with the ATLAS detector*, ATLAS-CONF-2016-051.
- [81] J. M. Campbell and R. K. Ellis, *$t\bar{t}W^{+-}$ production and decay at NLO*, *JHEP* **07** (2012) 052, [[1204.5678](#)].
- [82] A. Lazopoulos, T. McElmurry, K. Melnikov and F. Petriello, *Next-to-leading order QCD corrections to $t\bar{t}Z$ production at the LHC*, *Phys. Lett.* **B666** (2008) 62–65, [[0804.2220](#)].
- [83] S. Frixione, V. Hirschi, D. Pagani, H. S. Shao and M. Zaro, *Electroweak and QCD corrections to top-pair hadroproduction in association with heavy bosons*, *JHEP* **06** (2015) 184, [[1504.03446](#)].
- [84] T. Sjostrand, S. Mrenna and P. Z. Skands, *PYTHIA 6.4 Physics and Manual*, *JHEP* **05** (2006) 026, [[hep-ph/0603175](#)].
- [85] DELPHES 3 collaboration, J. de Favereau, C. Delaere, P. Demin, A. Giammanco, V. Lematre, A. Mertens et al., *DELPHES 3, A modular framework for fast simulation of a generic collider experiment*, *JHEP* **02** (2014) 057, [[1307.6346](#)].
- [86] M. Cacciari, G. P. Salam and G. Soyez, *The Anti- $k(t)$ jet clustering algorithm*, *JHEP* **04** (2008) 063, [[0802.1189](#)].

- [87] E. Conte, B. Fuks and G. Serret, *MadAnalysis 5, A User-Friendly Framework for Collider Phenomenology*, *Comput. Phys. Commun.* **184** (2013) 222–256, [[1206.1599](#)].
- [88] ATLAS collaboration, T. A. collaboration, *Calibration of the performance of b-tagging for c and light-flavour jets in the 2012 ATLAS data*, ATLAS-CONF-2014-046.
- [89] ATLAS collaboration, T. A. collaboration, *Measurement of the W^+W^- production cross section in pp collisions at a centre-of-mass energy of $\sqrt{s} = 13$ TeV with the ATLAS experiment*, ATLAS-CONF-2016-090.
- [90] ATLAS collaboration, T. A. collaboration, *Electron efficiency measurements with the ATLAS detector using the 2015 LHC proton-proton collision data*, ATLAS-CONF-2016-024.
- [91] ATLAS collaboration, G. Aad et al., *Muon reconstruction performance of the ATLAS detector in protonproton collision data at $\sqrt{s} = 13$ TeV*, *Eur. Phys. J.* **C76** (2016) 292, [[1603.05598](#)].
- [92] M. L. Mangano et al., *Physics at a 100 TeV pp Collider: Standard Model Processes*, *CERN Yellow Report* (2017) 1–254, [[1607.01831](#)].